

# An efficient preconditioning scheme for real-fluid mixtures using primitive pressure–temperature variables

NAN ZONG and VIGOR YANG\*

Department of Mechanical and Nuclear Engineering, The Pennsylvania State University, University Park, PA 16802, USA

(Received 16 February 2007; revised 30 April 2007; in final form 14 July 2007)

An improved preconditioning scheme incorporating a unified treatment of general fluid thermodynamics is developed for treating fluid flows over the entire regime of fluid thermodynamic states at all speeds. All of the thermodynamic and numerical properties (such as eigenvalues and Jacobian matrices) are derived directly from fundamental thermodynamics theories, rendering a self-consistent and robust algorithm. Further efficiency is obtained by employing temperature instead of enthalpy as the primary dependent variable in the preconditioned energy equation. No iterative solution of a real-fluid equation of state is required. This approach, combined with the use of explicit treatments of temporal and spatial derivatives, results in a scheme for which load balance is much easier to achieve in a distributed computing environment. A numerical stability analysis is performed to assess the effectiveness of the scheme at various fluid thermodynamic states. Sample calculations are also carried out. These include injection and mixing of cryogenic fluids and flame dynamics of coaxial jets of liquid oxygen and methane under supercritical conditions. The robustness and efficiency of the present work are demonstrated over a wide range of thermodynamic and flow conditions.

**Keywords:** Real-fluid thermodynamics; Supercritical fluid transport; All-speed fluid flow; Preconditioning method; General fluids

## 1. Introduction

The development of an efficient numerical algorithm capable of handling fluid flows over a broad range of thermodynamic states is of particular importance for many scientific and engineering problems. Notable examples include fluid transport, material processing, and combustion at high pressures. Thermodynamic non-idealities and transport anomalies often occur under these conditions, especially during the transition from a subcritical to a supercritical state (Yang 2000). Thus, treating fluid state transition and thermophysical-property variations in a manner consistent with the intrinsic characteristics of a numerical algorithm is critical to achieving numerical efficiency and robustness.

Several attempts have been made to treat fluid flows at different thermodynamic states. Merkle *et al.* (1998) extended a preconditioning scheme for ideal gases (Tukel 1987, Choi and Merkle 1993, Shuen *et al.* 1993, Weiss and Smith 1995, Darmofal and Van Leer 1998, Tukel 1999) to accommodate arbitrary equations of state. The resultant scheme, along with the use of the Soave–Redlich–Kwong

equation of state, has been employed to simulate supercritical hydrogen flow through a two-dimensional cascade and a heated rectangular duct. Although encouraging results were obtained for the specific problems considered, no information was given about the evaluation of thermophysical properties. The relationship between numerical properties and general fluid thermodynamics was not addressed.

Edwards *et al.* (2000) considered real-fluid flows with liquid–vapour phase transition using a low-diffusion flux-splitting scheme (Edwards and Liou 1998). The fluid  $p$ – $v$ – $T$  behaviour in the liquid phase was modelled with the Sanchez–Lacombe equation of state. A homogeneous vapour–liquid phase equilibrium model was employed to study the vapour cavitation during liquid carbon dioxide expansion through a sharp-orifice nozzle. Numerical experiments demonstrated the effectiveness of the method in capturing several important two-phase flow phenomena, such as cavitation bubbles and vapour–liquid condensation shocks. The scheme was later extended to investigate gas–solid two-phase flows in fluidized beds under different flow conditions (Mao *et al.* 2003).

\*Corresponding author. Tel.: + 1-814-863-1502. Fax: + 1-814-865-3389. Email: vigor@psu.edu

Oefelein and Yang (1998) extended the preconditioning methodology described in Hsieh and Yang (1997) to handle multi-component, dense-fluid mixtures with finite-rate chemical kinetics at supercritical pressures. Temporally accurate solutions were obtained through the implementation of a dual-time-stepping integration technique, in which the primitive variables of pressure, velocity components, temperature, and mass fraction were chosen as the dependent variables in pseudo-time. The Soave–Redlich–Kwong equation of state was employed to predict the fluid volumetric behaviour except in regions near the critical point, for which the Benedict–Webb–Rubin equation of state was used. Thermodynamic properties, such as the enthalpy, Gibbs energy, and specific heat, were obtained as explicit functions of temperature and pressure by using Maxwell's relations to derive thermodynamic departure functions (Yang 2000). Transport properties were estimated using an extended corresponding-state principle. The combined theoretical/numerical framework was applied to study the mixing and combustion of cryogenic propellants in supercritical environments (Oefelein and Yang 1998, Oefelein 2006). The properties of fluid mixtures (i.e. enthalpy and internal energy) in their analysis, however, were evaluated with the formulas for an ideal gas mixture, taking as the mass-weighted sum of the values of constituent species without considering their interactions. Since the coupling between molecules of different species may be significant in real-fluids, such a simplification leads to inconsistency with real-fluid equations of state and other property evaluation schemes.

To remedy this deficiency, Meng and Yang (2003) developed a unified numerical treatment of general fluid thermodynamics. The concepts of partial-mass and partial-density were introduced to evaluate the properties of real-fluid mixtures. All of the thermodynamic properties and numerical relations, including the Jacobian matrices and eigenvalues, were derived directly from fundamental thermodynamics theories, rendering a self-consistent and robust algorithm valid over the entire range of fluid states. Furthermore, full account is taken of transport property variations as functions of fluid density, temperature, and composition. The resultant numerical properties and property evaluation routines were incorporated into a preconditioning scheme (Hsieh and Yang 1997) to handle fluid flows at all speeds. The overall approach is general and can accommodate any type of equation of state.

In spite of its effectiveness in treating real-fluid flows with thermodynamic non-idealities and transport anomalies (Meng and Yang 2003, Meng *et al.* 2005), the aforementioned formulation cannot, in general, be solved in a non-iterative manner because the specific enthalpy is used as one of the dependent variables in the formulation of the pseudo-time derivatives. Extensive iterations at each time step and grid point are required to determine the fluid temperature from the specific enthalpy. Although such iterations are straightforward to handle for an ideal

gas mixture, the procedure becomes quite complicated and time-consuming for real-fluid mixtures due to the complicated form of the equation of state and property evaluation schemes. The iterative solution of a real-fluid equation of state not only significantly increases the computational cost, but also impairs the scalability of a parallelized code.

The purpose of the present work is to circumvent this limitation by replacing specific enthalpy with temperature as a primary dependent variable in the numerical formulation. Such an employment of the pressure–temperature type of primitive variables has been made in many existing approaches (Turkel 1987, Choi and Merkle 1993, Shuen *et al.* 1993, Weiss and Smith 1995, Darmofal and Van Leer 1998, Turkel 1999) and offers the following advantageous. First, laborious iterations in calculating temperature from specific enthalpy or internal energy are avoided, rendering a highly efficient algorithm for real-fluid mixtures. Second, load balance is easier to achieve on a distributed computing facility, since no iterative solution of the equation of state is required. The computation burden at each spatial grid point is the same. Third, computation of numerical Jacobian matrices is simplified, especially within the context of the general fluid thermodynamics. In addition, the preconditioning matrix in this study is derived by analysing the eigenvalues of the governing system. All the off-diagonal terms in the Jacobian matrix relating the conservative to preconditioning variables are retained. The original governing equations can thus be fully recovered for high-speed flows in a steady state simulation. The scheme is further optimized to facilitate parallel computation by treating the pseudo-time and spatial derivatives using a fourth-order Runge-Kutta (RK4) scheme (Jameson 1983) and an explicit fourth-order flux-differencing scheme (Rai and Chakravarthy 1993), respectively. Because the time advancement is fully explicit in the pseudo-time space, the approach not only guarantees high-order numerical accuracy in both time and space, but also simplifies the implementation of a parallelized code.

The remainder of this paper is organized as follows. In Section 2, we briefly summarize the theoretical framework, including the governing equations and basic thermodynamics theories for general fluid mixtures. Fundamental thermodynamic and numerical attributes are established. Section 3 deals with the numerical implementation of the present scheme. A stability analysis is carried out in Section 4 to characterize the stability and convergence behaviour of the algorithm. Section 5 presents results from selected numerical experiments, along with an assessment of the computational efficiency. Finally, a brief summary concludes the work.

## 2. Theoretical formulation

To facilitate discussion, we consider the two-dimensional conservation equations of mass, momentum, energy, and

species transport for a chemically reacting system of  $N$  species. Following the approach detailed in Shuen *et al.* (1993) and Weiss and Smith (1995) for developing a preconditioning scheme for fluid flows at all speeds, a pseudo-time derivative of the form  $\Gamma \partial \hat{Q} / \partial \tau$  is added to the conservation equations,

$$\Gamma \frac{\partial \hat{Q}}{\partial \tau} + \frac{\partial Q}{\partial t} + \frac{\partial(E - E_v)}{\partial x} + \frac{\partial(F - F_v)}{\partial y} = S \quad (2.1)$$

where  $\Gamma$  represents the preconditioning matrix and  $\tau$  the pseudo-time. The conservative variable vector,  $Q$ , is defined as,

$$Q = y^\delta [\rho \quad \rho u \quad \rho v \quad \rho e_t \quad \rho Y_i]^T. \quad (2.2)$$

The exponent  $\delta = 0$  or  $1$  corresponds to a planar two-dimensional or an axisymmetric case, respectively. Standard notations in fluid mechanics are used here, with  $\rho$ ,  $(u, v)$ ,  $e_t$ , and  $Y_i$  denoting the density, velocity components, specific total energy, and mass fraction of species  $i$ , respectively. Explicit expressions of the convective flux vectors,  $E$  and  $F$  and the diffusion flux vectors,  $E_v$  and  $F_v$ , are given in Hsieh (1997), Meng and Yang (2003), Oefelein (2006). The source term in equation (2.1),  $S$ , arises from chemical reactions or axisymmetric geometry (Hsieh 1997).

Because the pseudo-time derivative in equation (2.1) vanishes at convergence, a certain amount of liberty can be taken in the selection of the pseudo-time variables (Tukel 1999). Different options have been proposed for the primary dependent variables in the preconditioning scheme for ideal gases. Those include conservative and several sets of primitive (e.g. pressure–entropy, pressure–enthalpy, and pressure–temperature) variables (Tukel 1999). The influences of selected preconditioning variables on the numerical convergence and accuracy for low Mach number aerodynamic problems were examined by Tukel (2002), Tukel and Vatsa (2003). Results indicated that the pressure–temperature type of primitive variables, which has long been a favourable choice by many researchers, led to fast convergence for simulating steady state flows. The present study follows the same approach, and the pseudo-time variable vector,  $\hat{Q}$ , is thus defined as

$$\hat{Q} = [p_g, u, v, T, Y_i]. \quad (2.3)$$

The use of the gauge pressure,  $p_g$ , taken as the static pressure subtracted by a reference pressure (Shuen *et al.* 1993, Hsieh and Yang 1997), is crucial for two reasons. First, it allows the vectors  $E$ ,  $F$ ,  $E_v$ ,  $F_v$ , and  $S$  to be expressed as unique functions of  $\hat{Q}$  (Hsieh and Yang 1997). Second,  $p_g$  is much more sensitive to the solution than the density at low Mach numbers, and thus provides a stronger velocity–pressure coupling in the momentum balance. The selection of the velocity

components  $(u, v)$ , temperature,  $T$ , and species mass fraction,  $Y_i$ , helps maintain the direction of the diffusion process, simplifies the structures of viscous vectors, and reduces the computational complexity (Choi and Merkle 1993). In contrast to the schemes with the pressure–enthalpy type of primitive variables, all the thermodynamic properties of pressure, temperature, and mass fraction are directly solved, thereby eliminating tedious iterative solutions of the equations of state.

## 2.1 Thermodynamic relations

To develop a robust numerical scheme in a manner consistent with real-fluid thermodynamics, all the numerical properties and relations, including the preconditioning matrix, Jacobian matrices and system eigenvalues, must be derived in accordance with fundamental thermodynamics theories described by Meng and Yang (2003). The procedure should conform to the concepts of partial-mass and partial-density properties for fluid mixtures, along with the use of an appropriate equation of state.

Four thermodynamic relationships beyond those established in Meng and Yang (2003) are needed to derive the numerical properties. Those equations define density, enthalpy, and internal energy as functions of such dependent variables as pressure, temperature, and mass fraction, and consequently can be used to determine the Jacobian matrices  $T \equiv \partial Q / \partial \hat{Q}$ ,  $A \equiv \partial E / \partial \hat{Q}$ ,  $B \equiv \partial F / \partial \hat{Q}$  and  $D \equiv \partial S / \partial \hat{Q}$  (see Appendix A), as well as the associated eigen-properties.

### 2.1.1 Pressure as function of density, temperature, and mass fraction.

The first relationship expresses pressure as a function of temperature, density, and mass fractions. For a general fluid mixture consisting of  $N$  species, each intensive thermodynamic property can be determined by the other  $N + 1$  properties of the mixture. This leads to the following expression:

$$p = p(T, \rho_i) \quad (2.4)$$

where  $i = 1, \dots, N$ . The differential form of equation (2.4) is

$$dp = \left( \frac{\partial p}{\partial T} \right)_{\rho_i} dT + \sum_{i=1}^N \left( \frac{\partial p}{\partial \rho_i} \right)_{T, \rho_{j \neq i}} d\rho_i. \quad (2.5)$$

We may change the summation on the right-hand side of equation (2.5) from 1 through  $N$  to 1 through  $N - 1$

to obtain the following relation:

$$\begin{aligned} dp &= \left( \frac{\partial p}{\partial T} \right)_{\rho_i} dT \\ &+ \sum_{i=1}^{N-1} \left[ \left( \frac{\partial p}{\partial \rho_i} \right)_{T, \rho_{j \neq i}} - \left( \frac{\partial p}{\partial \rho_N} \right)_{T, \rho_{j \neq N}} \right] d\rho_i \\ &+ \left( \frac{\partial p}{\partial \rho_N} \right)_{T, \rho_{j \neq N}} d\rho. \end{aligned} \quad (2.6)$$

Since  $\rho_i = \rho Y_i$ ,

$$d\rho_i = Y_i d\rho + \rho dY_i \quad (2.7)$$

substitution of equation (2.7) into equation (2.6) yields

$$dp = A_T dT + A_{Y_i} dY_i + A_\rho d\rho \quad (2.8)$$

where

$$A_T = \left( \frac{\partial p}{\partial T} \right)_{\rho_i} \quad (2.9a)$$

$$A_{Y_i} = \rho \left[ \left( \frac{\partial p}{\partial \rho_i} \right)_{T, \rho_{j \neq i}} - \left( \frac{\partial p}{\partial \rho_N} \right)_{T, \rho_{j \neq N}} \right] \quad (2.9b)$$

$$A_\rho = \left( \frac{\partial p}{\partial \rho} \right)_{T, Y_i} \quad (2.9c)$$

It has been shown in Meng and Yang (2003) that the speed of sound for a general fluid mixture can be expressed as

$$a^2 = \left( \frac{\partial p}{\partial \rho} \right)_{s, Y_i} = \frac{C_p}{C_v} \left( \frac{\partial p}{\partial \rho} \right)_{T, Y_i} = \gamma A_\rho \quad (2.10)$$

where  $C_p$  and  $C_v$  are constant-pressure and constant-volume specific heats, respectively, and  $\gamma$  is the ratio of specific heat.

**2.1.2 Internal energy as function of temperature, pressure, and mass fraction.** The second relationship expresses internal energy as a function of pressure, density, and mass fractions. We begin with the following functional relationship:

$$\rho e = \rho e(T, \rho_i) \quad (2.11)$$

where  $i = 1, \dots, N$  and  $e$  the specific internal energy. The differential form of equation (2.11) can be written as

$$d\rho e = \rho \left( \frac{\partial e}{\partial T} \right)_{\rho_i} dT + \sum_{i=1}^N \left( \frac{\partial \rho e}{\partial \rho_i} \right)_{T, \rho_{j \neq i}} d\rho_i. \quad (2.12)$$

The derivative in the first term on the right-hand side is the constant-volume heat capacity,  $C_v$ , and that in the second

term is the partial-density internal energy,  $\tilde{e}_i$  (Meng and Yang 2003),

$$\tilde{e}_i = \left( \frac{\partial \rho e}{\partial \rho_i} \right)_{T, \rho_{j \neq i}} \quad (2.13)$$

equation (2.12) thus becomes

$$d\rho e = \rho C_v dT + \sum_{i=1}^N \tilde{e}_i d\rho_i. \quad (2.14)$$

Substitution of equation (2.7) into equation (2.14) gives

$$d\rho e = \rho C_v dT + \sum_{i=1}^N \tilde{e}_i \rho dY_i + \sum_{i=1}^N \tilde{e}_i Y_i d\rho. \quad (2.15)$$

Since  $d\rho e = \rho de + e d\rho$ , a simple manipulation of equation (2.15) results in

$$\begin{aligned} de &= C_v dT + \sum_{i=1}^{N-1} (\tilde{e}_i - \tilde{e}_N) dY_i \\ &+ \frac{1}{\rho} \left( \sum_{i=1}^N Y_i \tilde{e}_i - e \right) d\rho. \end{aligned} \quad (2.16)$$

Substitution of equation (2.8) into the above equation leads to

$$de = B_T dT + B_p d\rho + \sum_{i=1}^{N-1} B_{Y_i} dY_i \quad (2.17)$$

where

$$B_T = C_v - \frac{1}{\rho} \left( \sum_{i=1}^N Y_i \tilde{e}_i - e \right) \left( \frac{\partial \rho}{\partial p} \right)_{T, Y_i} \left( \frac{\partial p}{\partial T} \right)_{\rho_i} \quad (2.18a)$$

$$B_p = \frac{1}{\rho} \left( \sum_{i=1}^N Y_i \tilde{e}_i - e \right) \left( \frac{\partial \rho}{\partial p} \right)_{T, Y_i} \quad (2.18b)$$

$$\begin{aligned} B_{Y_i} &= \left\{ (\tilde{e}_i - \tilde{e}_N) - \left( \sum_{i=1}^N Y_i \tilde{e}_i - e \right) \left( \frac{\partial \rho}{\partial p} \right)_{T, Y_i} \right. \\ &\quad \left. \times \left[ \left( \frac{\partial p}{\partial \rho_i} \right)_{T, \rho_{j \neq i}} - \left( \frac{\partial p}{\partial \rho_N} \right)_{T, \rho_{j \neq N}} \right] \right\}. \end{aligned} \quad (2.18c)$$

**2.1.3 Enthalpy as function of temperature, pressure, and mass fraction.** The third relationship expresses enthalpy as a function of pressure, temperature, and mass fractions. According to basic thermodynamic definitions,

we have

$$dh = de + \frac{1}{\rho} dp - \frac{p}{\rho^2} d\rho. \quad (2.19)$$

Substituting equations (2.8) and (2.17) into equation (2.19) and following some straightforward manipulations, we obtain

$$dh = D_T dT + D_p dp + \sum_{i=1}^{N-1} D_{Y_i} dY_i \quad (2.20)$$

where

$$D_T = C_v - \frac{1}{\rho} \left( \frac{\partial p}{\partial T} \right)_{\rho_i} \left( \frac{\partial \rho}{\partial p} \right)_{T, Y_i} \left( \sum_{i=1}^N Y_i \tilde{e}_i - e - \frac{p}{\rho} \right) \quad (2.21a)$$

$$D_p = \frac{1}{\rho} + \frac{1}{\rho} \left( \frac{\partial \rho}{\partial p} \right)_{T, Y_i} \left( \sum_{i=1}^N Y_i \tilde{e}_i - e - \frac{p}{\rho} \right) \quad (2.21b)$$

$$D_{Y_i} = \tilde{e}_i - \tilde{e}_N - \left( \frac{\partial \rho}{\partial p} \right)_{T, Y_i} \left( \sum_{i=1}^N Y_i \tilde{e}_i - e - \frac{p}{\rho} \right) \times \left[ \left( \frac{\partial p}{\partial \rho_i} \right)_{T, \rho_j \neq i} - \left( \frac{\partial p}{\partial \rho_N} \right)_{T, \rho_j \neq N} \right]. \quad (2.21c)$$

The coefficient,  $D_T$ , is equivalent to the constant-pressure heat capacity,  $C_p$ , of a fluid mixture, according to its definition. Thus,

$$C_p = D_T = C_v - \frac{1}{\rho} \left( \frac{\partial p}{\partial T} \right)_{\rho_i} \left( \frac{\partial \rho}{\partial p} \right)_{T, Y_i} \left( \sum_{i=1}^N Y_i \tilde{e}_i - e - \frac{p}{\rho} \right). \quad (2.22)$$

**2.1.4 Relationship between constant-pressure and constant-volume specific heats.** The final relationship deals with constant-pressure and constant-volume specific heats. According to fundamental thermodynamics for a multi-component mixture,

$$s = s(T, \rho, Y_i) \quad i = 1, \dots, N-1. \quad (2.23)$$

Its differential form can be written as

$$ds = \frac{C_v}{T} dT + \left( \frac{\partial s}{\partial \rho} \right)_{T, Y_i} d\rho + \sum_{i=1}^{N-1} \left( \frac{\partial s}{\partial Y_i} \right)_{T, \rho, Y_{j \neq i}} dY_i. \quad (2.24)$$

A similar relationship that defines entropy as a function of temperature, pressure, and mass fraction can be easily

derived as

$$ds = \frac{C_p}{T} dT + \left( \frac{\partial s}{\partial p} \right)_{T, Y_i} dp + \sum_{i=1}^{N-1} \left( \frac{\partial s}{\partial Y_i} \right)_{T, \rho, Y_{j \neq i}} dY_i. \quad (2.25)$$

Combination of equations (2.24) and (2.25) and rearrangement of the result lead to

$$\left( \frac{C_p}{T} - \frac{C_v}{T} \right) dT = \left( \frac{\partial s}{\partial \rho} \right)_{T, Y_i} d\rho - \left( \frac{\partial s}{\partial p} \right)_{T, Y_i} dp + \sum_{i=1}^{N-1} \left[ \left( \frac{\partial s}{\partial Y_i} \right)_{T, \rho, Y_{j \neq i}} - \left( \frac{\partial s}{\partial Y_i} \right)_{T, p, Y_{j \neq i}} \right] dY_i. \quad (2.26)$$

Substitution of equation (2.8) into equation (2.26) and elimination of  $dp$  give,

$$\left[ \frac{C_p}{T} - \frac{C_v}{T} + \left( \frac{\partial s}{\partial p} \right)_{T, Y_i} \left( \frac{\partial p}{\partial T} \right)_{T, Y_i} \right] dT = \left[ \left( \frac{\partial s}{\partial \rho} \right)_{T, Y_i} - \left( \frac{\partial s}{\partial p} \right)_{T, Y_i} \left( \frac{\partial p}{\partial \rho} \right)_{T, Y_i} \right] d\rho + \sum_{i=1}^{N-1} \left[ \left( \frac{\partial s}{\partial Y_i} \right)_{T, \rho, Y_{j \neq i}} - \left( \frac{\partial s}{\partial Y_i} \right)_{T, p, Y_{j \neq i}} - \left( \frac{\partial s}{\partial p} \right)_{T, Y_i} \left( \frac{\partial p}{\partial Y_i} \right)_{T, Y_{j \neq i}} \right] dY_i. \quad (2.27)$$

Since temperature, density, and mass fraction can vary independently, the coefficients of the above differentials must vanish. Thus,

$$C_p = C_v - T \left( \frac{\partial s}{\partial p} \right)_{T, Y_i} \left( \frac{\partial p}{\partial T} \right)_{\rho, Y_i}. \quad (2.28)$$

Application of the well-known Maxwell relation (Moran and Shapiro 1999),

$$\left( \frac{\partial s}{\partial p} \right)_{T, Y_i} = \frac{1}{\rho^2} \left( \frac{\partial \rho}{\partial T} \right)_{p, Y_i} = \frac{-\frac{1}{\rho^2} \left( \frac{\partial \rho}{\partial T} \right)_{\rho, Y_i}}{\left( \frac{\partial \rho}{\partial \rho} \right)_{T, Y_i}} \quad (2.29)$$

gives,

$$C_p = C_v + \frac{T}{\rho^2} \frac{\left( \frac{\partial \rho}{\partial T} \right)_{\rho_i}^2}{\left( \frac{\partial \rho}{\partial \rho} \right)_{T, Y_i}}. \quad (2.30)$$

This relationship will be employed to calculate the eigenvalues of the preconditioned governing system.

## 2.2 Preconditioning matrix

The precondition matrix  $\Gamma$  in equation (2.1) is introduced to rescale the system eigenvalues in such a manner that they have the same order of magnitude to ensure uniform convergence at all Mach numbers. The specific form of the matrix is not unique (Tukel 1999), and is selected to maximize the numerical efficiency over a broad range of flow conditions. Generally, this matrix can be constructed by means of either an eigenvalue analysis (Tukel 1987, 1999) or an asymptotic theory (Guillard and Viozat 1999, Venkateswaran *et al.* 2004).

Following the standard approach suggested in Choi and Merkle (1993), we examine the Jacobian matrix  $T \equiv \partial Q / \partial \hat{Q}$  in Appendix A. A common term  $(\partial \rho / \partial p)_{T, Y_i}$ , which can be expressed as

$$\left( \frac{\partial \rho}{\partial p} \right)_{T, Y_i} = \frac{C_p}{C_v} \left( \frac{\partial \rho}{\partial p} \right)_{s, Y_i} = \frac{\gamma}{a^2} \quad (2.31)$$

is identified in each element of the first column of  $T$ . It is this term, after multiplication of the time derivatives of dependent variables in equation (2.1), that dictates the propagation speeds of acoustic waves in the governing system (Choi and Merkle 1993). The preconditioning matrix is, then, established by simply replacing this term with a scaling factor,  $\Theta$ .

$$\Gamma = \begin{pmatrix} \Theta & 0 & 0 & -\frac{A_T}{A_\rho} & -\frac{A_{Y_1}}{A_\rho} & \dots & -\frac{A_{Y_{N-1}}}{A_\rho} \\ \Theta u & \rho & 0 & -\frac{A_T u}{A_\rho} & -\frac{A_{Y_1} u}{A_\rho} & \dots & -\frac{A_{Y_{N-1}} u}{A_\rho} \\ \Theta v & 0 & \rho & -\frac{A_T v}{A_\rho} & -\frac{A_{Y_1} v}{A_\rho} & \dots & -\frac{A_{Y_{N-1}} v}{A_\rho} \\ \Theta h_t + \left( \sum_{i=1}^N Y_i \tilde{e}_i - e - \frac{p}{\rho} \right) \left( \frac{\partial \rho}{\partial p} \right)_{T, Y_i} & \rho u & \rho v & \rho B_T - \frac{A_T e_t}{A_\rho} & \rho B_{Y_1} - \frac{A_{Y_1} e_t}{A_\rho} & \dots & \rho B_{Y_{N-1}} - \frac{A_{Y_{N-1}} e_t}{A_\rho} \\ \Theta Y_1 & 0 & 0 & -\frac{A_T Y_1}{A_\rho} & \rho - \frac{A_{Y_1} Y_1}{A_\rho} & \dots & -\frac{A_{Y_{N-1}} Y_1}{A_\rho} \\ \vdots & \vdots & \vdots & \vdots & \vdots & \ddots & \vdots \\ \Theta Y_{N-1} & 0 & 0 & -\frac{A_T Y_{N-1}}{A_\rho} & -\frac{A_{Y_1} Y_{N-1}}{A_\rho} & \dots & \rho - \frac{A_{Y_{N-1}} Y_{N-1}}{A_\rho} \end{pmatrix} \quad (2.32)$$

where the two sets of coefficients  $(A_T, A_\rho, A_{Y_i})$  and  $(B_T, B_{Y_i})$  are defined by equations (2.9) and (2.18), respectively. The scaling factor,  $\Theta$ , is defined as,

$$\Theta = [1/\varepsilon^2 + (\gamma - 1)]/a^2. \quad (2.33)$$

The preconditioning factor,  $\varepsilon$ , lies between 0 and 1. In comparison with the preconditioning matrices defined in Choi and Merkle (1993), Shuen *et al.* (1993), Hsieh and Yang (1997), Meng and Yang (2003), all of the off-diagonal terms in equation (2.32) are retained. The preconditioning matrix becomes the Jacobian matrix  $T \equiv \partial Q / \partial \hat{Q}$  in the limit of  $\varepsilon \rightarrow 1$ , and the original governing system is recovered for high-speed flows in a steady state simulation. For an ideal gas, the preconditioning matrix,  $\Gamma$ , reduces to the form introduced by Weiss and Smith (1995), and becomes a member of the generalized preconditioner family suggested

by Tukel (1987, 1999). For an incompressible fluid, as the speed of sound,  $a$ , reaches infinite, the preconditioning matrix takes a form similar to that proposed in Choi and Merkle (1993). As will be shown later, through an appropriate selection of the preconditioning factor,  $\varepsilon$ , the preconditioning matrix developed herein can effectively circumvent the eigenvalue-disparity problem associated with low Mach number flows and help achieve an optimal convergence rate in the entire flowfield.

According to Choi and Merkle (1993), the preconditioning factor for an inviscid flow is specified as

$$\varepsilon_{\text{inv}} = \begin{cases} \varepsilon_{\text{min}} & M \leq \varepsilon_{\text{min}} \\ M^2 & \varepsilon_{\text{min}} < M < 1 \\ 1 & M \geq 1. \end{cases} \quad (2.34)$$

A lower bound,  $\varepsilon_{\text{min}}$ , typically taken as  $10^{-5}$ , is used to avoid the singularity of a stagnation point. In regions where diffusion plays a dominant role in determining the flow behaviour, it is important to simultaneously control both the Courant–Friedriches–Lewy (CFL) and von Neumann (VNN) numbers to achieve efficient convergence (Buelow *et al.* 1994). Oefelein and Yang (1998) suggested that the viscous preconditioning factor,  $\varepsilon_{\text{vis}}$ , be selected as

$$\varepsilon_{\text{vis}} = \max \left[ \frac{u^2 \delta_x (\delta_x - 1)}{u^2 \delta_x^2 + a^2}, \frac{v^2 \delta_y (\delta_y - 1)}{v^2 \delta_y^2 + a^2} \right] \quad (2.35)$$

where

$$\delta_x = \max \left( v, \frac{v}{Pr}, \frac{v}{Sc_i} \right) \frac{1}{u} \frac{\text{CFL}}{\text{VNN}} \quad (2.36)$$

$$\delta_y = \max \left( v, \frac{v}{Pr}, \frac{v}{Sc_i} \right) \frac{1}{v} \frac{\text{CFL}}{\text{VNN}}$$

and  $\nu$ ,  $Pr$ , and  $Sc_i$  are the kinematic viscosity, cell Prandtl number, and cell Schmidt number of species  $i$ , respectively.

equation (2.36) takes into account the effects of momentum, energy, and mass diffusion on the overall convergence rate.

A preconditioning factor that can optimally control both convection and diffusion processes is determined locally as

$$\varepsilon = \min[1, \max(\varepsilon_{\text{inv}}, \varepsilon_{\text{vis}})]. \quad (2.37)$$

### 2.3 System eigenvalues

The basic characteristics of the algorithm developed herein, specifically, the numerical convergence and stability properties, can be examined by studying the system eigenvalues. For brevity, only those eigenvalues associated with the inviscid flux vector in the axial direction,  $\Gamma^{-1}A$  with  $A \equiv \partial E / \partial \hat{Q}$ , are discussed.

$$\lambda_A = \text{diag}(\lambda_1 \quad \lambda_2 \quad u \quad u \quad \dots \quad u) \quad (2.38)$$

where  $\lambda_1$  and  $\lambda_2$  represent the rescaled acoustic wave speeds propagating upstream and downstream, respectively,

$$\lambda_{1,2} = \frac{1}{2} \left[ (q_{11} + u) \pm \sqrt{(q_{11} - u)^2 - 4(uq_{11} - \varepsilon a^2)} \right]. \quad (2.39)$$

The variable  $q_{11}$  represents the first element in the first column of the matrix,  $\Gamma^{-1}A$ .

$$q_{11} = \frac{u \left( \frac{\gamma C_p}{a^2} - \frac{T A_T^2}{\rho^2 A_p^2} \right)}{\left( \frac{\gamma C_p}{\beta} - \frac{T A_T^2}{\rho^2 A_p^2} \right)} \quad (2.40)$$

where  $A_T$  and  $A_p$  are given in equations (2.9a) and (2.9c), respectively. We then obtain,

$$\frac{A_T^2}{A_p^2} = \frac{\left( \frac{\partial p}{\partial T} \right)_{\rho_i}^2}{\left( \frac{\partial p}{\partial \rho} \right)_{T, Y_i}^2}. \quad (2.41)$$

Combination of equations (2.41) and (2.30) and substitution of equation (2.10) into the resultant equation yield

$$C_p = C_v + \frac{T}{\rho^2} \cdot \frac{A_T^2}{A_p^2} \cdot \frac{C_v}{C_p} a^2. \quad (2.42)$$

The above equation can be rearranged to become

$$\frac{A_T^2}{A_p^2} = \frac{\rho^2 (\gamma - 1) C_p}{T a^2}. \quad (2.43)$$

Incorporation of equation (2.43) into equation (2.40) leads to

$$q_{11} = \frac{u \left( \frac{\gamma C_p}{a^2} - \frac{T A_T^2}{\rho^2 A_p^2} \right)}{\left( \frac{\gamma C_p}{\beta} - \frac{T A_T^2}{\rho^2 A_p^2} \right)} = \varepsilon u. \quad (2.44)$$

The first two system eigenvalues,  $\lambda_{1,2}$ , can thus be obtained by substituting equation (2.44) into equation (2.39).

$$\lambda_{1,2} = \frac{1}{2} \left[ (1 + \varepsilon)u \pm \sqrt{(1 - \varepsilon)^2 u^2 + 4\varepsilon a^2} \right]. \quad (2.45)$$

All of the eigenvalues in the pseudo-time space are real, and have signs consistent with the directions of characteristic wave propagation. The present scheme not only preserves the hyperbolicity of the system, but also gives rise to individual eigenvalues that behave in a manner representative of the physical reality involved (Hsieh and Yang 1997). The same conclusion was reached in Meng and Yang (2003) using different pseudo-time variables and preconditioning matrix.

### 3. Numerical implementation

A dual-time-stepping integration technique is implemented to obtain time-accurate results (Shuen *et al.* 1993, Hsieh and Yang 1997, Oefelein and Yang 1998, Meng and Yang 2003). The solution converged in pseudo-time corresponds to a time-accurate solution in physical time. One major advantage of this technique lies in the fact that the convergence of the iterative process is dictated by the well-behaved eigenvalues in the pseudo-time space, instead of the original eigenvalues that may become disparate in certain flow regimes (e.g. low Mach number flows; Shuen *et al.* 1993).

A standard fourth-order Runge-Kutta (RK4) scheme (Jameson 1983) is employed to perform the inner-loop pseudo-time integration because of its relatively higher temporal accuracy and greater stability margin compared to many commonly used explicit schemes. The temporal discretization of the real-time derivative term is obtained using a second-order backward difference. Spatial discretization is achieved by means of a fourth-order flux-differencing scheme (Rai and Chakravarthy 1993). Further improvement is acquired by adding both the second- and fourth-order artificial dissipation with a total-variation-diminish (TVD) switch (Swanson and Turkel 1992, Jorgenson and Turkel 1993) to ensure numerical stability and convergence. The former is enforced only in regions with strong gradients, whereas the latter is applied in smooth regimes to achieve numerical stability. The details about implementation of artificial dissipation in a preconditioning scheme can be found in Turkel (1999).

Because the time advancement is fully explicit in pseudo-time and only the neighbouring data at the previous time step is required when evaluating the derivatives of the convective and viscous terms, the present scheme is suitable for parallel implementation. The scheme is then parallelized using a multiblock domain decomposition technique with message passing interfaces (MPI) at the domain boundaries. The parallelization methodology is robust and the speedup is almost linear.

#### 4. Stability analysis

A VNN analysis is performed to characterize the stability and convergence behaviour of the present scheme. For simplicity, only the inviscid part without any source terms is considered, and the coefficient matrices are assumed to be locally constant. The amplification matrix is obtained by the Fourier transformation of the discretized governing equations to the wave-number space. The partial derivatives of the thermodynamic properties in the corresponding numerical Jacobian matrices and the fluid  $p$ - $v$ - $T$  behaviour are evaluated with a modified Soave-Redlich-Kwong equation of state (Graboski and Daubert 1978, 1979).

Figure 1(a) shows the one-dimensional stability characteristics for an ideal gas in terms of the magnitude of the largest eigenvalue of the amplification matrix. The numerical parameters are  $CFL = 0.7$ ,  $\Delta\tau/\Delta t = 1$ , and  $\varepsilon_x^{(4)} = 1/64$ , where the latter denotes the coefficient of the fourth-order artificial dissipation. The result of the RK4 integration combined with the fourth-order central differencing (4CD) scheme is also included for comparison. The amplification factor of the standard RK4-4CD algorithm approaches unity in the bulk of the wave-number space, whereas the preconditioning technique stabilizes numerical calculations over the entire domain at all Mach numbers.

The effects of fluid state on the numerical stability behaviour are investigated by considering nitrogen fluid at a near-critical ( $p = 40$  atm and  $T = 120$  K), a transcritical ( $p = 90$  atm and  $T = 120$  K), and a supercritical ( $p = 90$  atm and  $T = 185$  K), fluid state. Table 1 lists the thermodynamic critical properties of nitrogen.

The compressibility-factors,  $Z$ , which measure the departure from the ideal gas behaviour, are 0.2, 0.4, and 0.8 at those three different fluid states, respectively. As evidenced in figure 1(b), the present scheme appears to be quite robust and exhibits an almost identical stability behaviour independent of fluid states. The same result is obtained for all flow Mach numbers.

Two-dimensional stability analyses are also conducted for an ideal gas, a cryogenic oxygen fluid ( $p = 100$  atm and  $T = 100$  K), and a supercritical fluid mixture of oxygen and methane ( $p = 100$  atm,  $T = 200$  K and  $x_{O_2} = 0.5$ ) at a flow Mach number of  $10^{-3}$  and a flow angle of 45 deg (i.e.  $v/u = 1$ ). The compressibility-factors for the latter two cases are 0.34 and 0.48, respectively. The amplification factors shown in figure 2 indicate that the scheme exhibits an identical stability behaviour in a two-dimensional domain, regardless of the fluid state. The result further corroborates the numerical uniformity and self-consistence of the general fluid thermodynamics treatment (Meng and Yang 2003) implemented herein.

#### 5. Sample calculations

The numerical scheme developed in the preceding sections has been applied to study a wide variety of flow problems in order to assess its accuracy, efficiency, and robustness. This section presents some representative results, including injection of cryogenic fluids and mixing and combustion of coaxial oxygen/methane fluid jets under supercritical conditions. For all the demonstration cases considered herein, turbulence closure is achieved by means of a large-eddy-simulation (LES) technique, in which large-scale motions are calculated explicitly and the effects of unresolved small-scale turbulence are modelled either analytically or empirically. The Favre-filtered mass, momentum, energy, and species conservation equations are derived by filtering small-scale dynamics from resolved scales over a well-defined set of spatial and temporal intervals. The effects of subgrid-scale (sgs) motions are treated using the model proposed by Erlebacher *et al.* (1992). It employs a Favre-averaged generalization of the Smagorinsky eddy-viscosity model coupled with a gradient-diffusion assumption to simulate

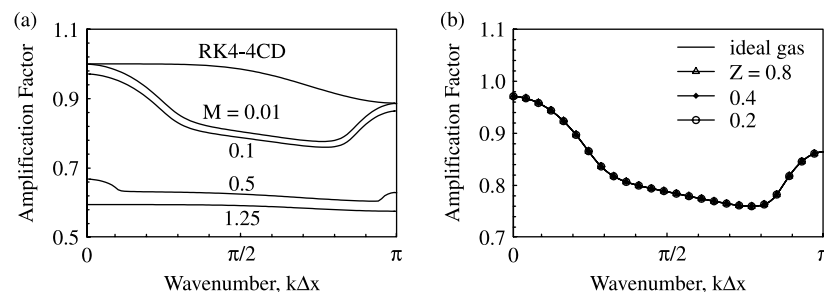


Figure 1. Amplification factor showing the one-dimensional stability characteristics of the scheme at  $CFL = 0.95$ ,  $\Delta\tau/\Delta t = 1$ ,  $\varepsilon_4 = 1/64$ , (a) ideal gas at  $M = 10^{-3}$ ,  $10^{-2}$ , 0.1 and 1.25; and (b) compressed nitrogen fluid at  $M = 0.1$  and  $Z = 0.2, 0.4, 0.8$ .

Table 1. Critical properties of nitrogen, methane, and oxygen.

	$p_c$ (atm)	$T_c$ (K)	$v_c$ (L/mol)
Nitrogen	34	126	0.089
Methane	46	190	0.099
Oxygen	50	154	0.076

sgs energy and species transport processes. The Smagorinsky coefficients  $C_R$  ( $\approx 0.01$ ) and  $C_I$  ( $\approx 0.007$ ) are determined empirically. Thermodynamic properties, such as enthalpy, Gibbs energy, and constant-pressure specific heat, are obtained directly from fundamental thermodynamics theories and a modified Soave–Redlich–Kwong equation of state (Graboski and Daubert 1978, 1979). Transport properties, such as viscosity and thermal conductivity, are evaluated using an extended corresponding-state theory (Ely and Hanley 1981, 1983) along with the 32-term Benedict–Webb–Robin equation of state (Jacobsen and Stewart 1973). Mass diffusivity is obtained by means of the Takahashi (1974) method, calibrated for high pressure conditions. The implementation and validation of the property evaluation schemes were detailed by Yang (2000) and Meng *et al.* (2005).

### 5.1 Cryogenic nitrogen fluid jet dynamics

The first case deals with the injection of cryogenic fluids into supercritical environments. Liquid nitrogen at a temperature of 120 K is injected through a circular tube with a diameter of 254  $\mu\text{m}$  into a supercritical nitrogen environment. A turbulent pipe flow with a bulk velocity of 15 m/s is assumed at the injector exit. The ambient temperature remains at 300 K, but the pressure varies from 69 to 93 atm, which is comparable to the chamber pressures of many operational rocket engines. Two different flow conditions summarized in table 2 are considered, simulating the experiments conducted by Chehroudi *et al.* (2002a,b). The subscripts  $\infty$  and inj

denote the injection and ambient conditions, respectively. The Reynolds number is defined as  $Re = \rho_{inj} u_{inj} D_{inj} / \mu_{inj}$ .

The computational domain downstream of the injector measures a length of  $40D_{inj}$  and a diameter of  $12D_{inj}$ . The dimensions are sufficient to minimize the effect of the far-field boundary conditions on the near-injector flow evolution. A three-dimensional grid consisting of  $225 \times 90 \times 72$  cells is employed. The mean grid size falls roughly in the inertial sub-range of the turbulent kinetic energy (TKE) spectrum, estimated using the Kolmogorov–Obukhov theory. The computational domain is divided into 54 blocks, with each calculated on a single processor of a distributed-memory parallel computer. The physical time step is  $1 \times 10^{-3}$  ms and the maximum CFL number for the inner-loop pseudo-time integration is 0.7. For each case, the calculation is first conducted for an extended period until the flowfield reaches its stationary state. The time stamp is then reset, and data is collected for more than 12 flow through times (i.e. 15 ms) to obtain statistically meaningful turbulence properties.

Figure 3 shows snapshots of the density-gradient fields at two different ambient pressures of 6.9 and 9.3 MPa. The salient features of supercritical fluid jets are well captured. The fluid state changes continuously from the injected liquid phase to the warmer ambient gas phase with a series of finger- or thread-like entities emerging from the jet surface and dissolving gradually in the surrounding gases. Strong anisotropy of turbulence occurs close to the jet interface, where large eddies of integral-length scales become flattened, and the radial component of the TKE is transferred to its axial quantity (Zong *et al.* 2004). Compared with incompressible turbulent jets, both vortex roll-up and pairing are delayed, which leads to a longer potential core, around  $8D_{inj}$  for Case 1. The influence of the density stratification decays as the ambient pressure increases. Thus, the location of vortex roll-up shifts upstream from  $x/D_{inj} \approx 5$  in Case 1 to  $x/D_{inj} \approx 3$  in Case 2, and the jet spreads wider and the length of the potential core reduces to  $6 - 7D_{inj}$  in the latter case.

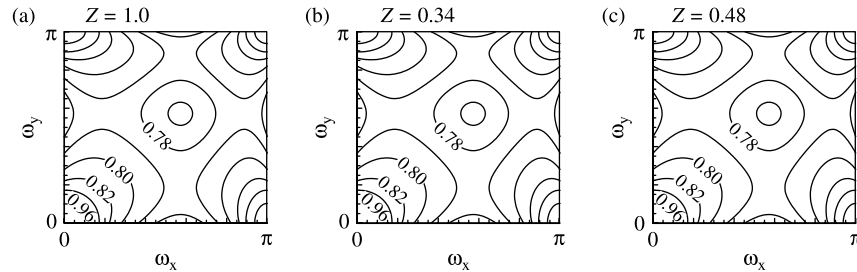


Figure 2. Amplification factors showing the two-dimensional stability characteristics of the scheme at  $M = 10^{-3}$ ,  $CFL = 0.95$  and  $\Delta\tau/\Delta t = 1$ , (a) ideal gas,  $Z = 1.0$ ; (b) compressed cryogenic oxygen at 100 K and 100 atm,  $Z = 0.34$ ; (c) supercritical oxygen/methane mixture at 200 K, 100 atm and oxygen mole fraction of 0.5,  $Z = 0.48$ .

Table 2. Simulation conditions for injection of liquid nitrogen.

	$p_\infty$ (MPa)	$T_{inj}$ (K)	$T_\infty$ (K)	$\rho_{inj}$ ( $\text{kg}/\text{m}^3$ )	$\rho_\infty$ ( $\text{kg}/\text{m}^3$ )	$\rho_{inj}/\rho_\infty$	$u_{inj}$ (m/s)	$M_{inj}$	$Re$
Case 1	6.9	120	300	603	77	7.83	15	0.031	44,700
Case 2	9.3	120	300	626	103	6.07	15	0.028	42,300

oxygen mole fraction of 0.5,  $Z = 0.48$ .

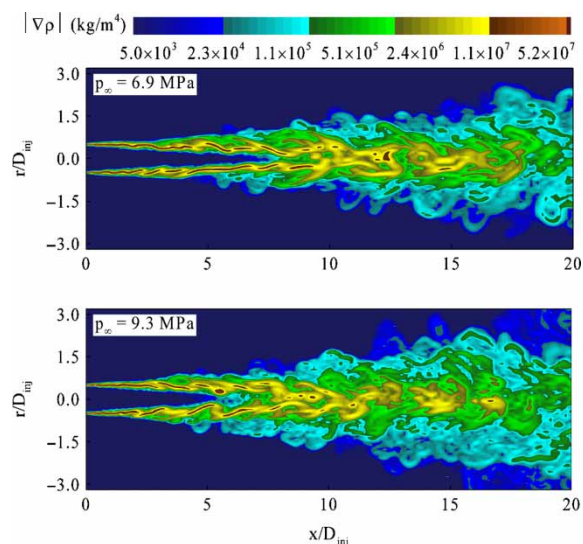


Figure 3. Effect of pressure on the density-gradient magnitude field ( $T_\infty = 300$  K,  $u_{inj} = 15$  m/s,  $T_{inj} = 120$  K,  $D_{inj} = 254$   $\mu$ m).

Figure 4 shows the radial distributions of the normalized mean density,  $\rho^* = (\bar{\rho} - \bar{\rho}_\infty)/(\bar{\rho}_c - \bar{\rho}_\infty)$ , at different axial locations. The radial coordinate is normalized by the full width of the radial profile measured where the fluid density is one half of its maximum value (FWHM),  $r_{1/2}$ , at the axial position of concern. Three distinct flow regimes, similar to incompressible turbulent jets, are identified. The potential core is manifested by the flat-hat distribution near the injector. The density profiles merge into a single distribution farther downstream ( $x/D_{inj} > 30$ ), which suggests the existence of a fully developed self-similarity region. A transition region occurs between 10 and  $30D_{inj}$ . The experimental data obtained using the Raman scattering technique at the test condition of Case 1 (Chehroudi *et al.* 2002a,b) is also plotted for comparison. Good agreement between calculations and measurements is achieved with a maximum deviation of 8%.

## 5.2 Supercritical mixing and combustion of oxygen and methane

The second case treats the flow and flame dynamics of a shear-coaxial injector operating at supercritical conditions, as shown schematically in figure 5. Co-flowing methane and oxygen streams are injected through two concentric tubes. The inner diameters of the Liquid oxygen (LOX) post and the methane annulus are 3.42 and 5.18 mm, respectively. Fully developed turbulent pipe flows are assumed at the injector exit. In the cold-flow simulations, supercritical oxygen and methane are injected at temperatures of 200 and 300 K, respectively. The bulk velocities of the two streams are 10 and 30 m/s, respectively.

The computational domain extends  $40\delta$  downstream of the injector exit with a radius of  $12\delta$ , where  $\delta$  is the thickness of the LOX post. A quasi-axisymmetric simulation involving  $360 \times 200$  grid points was conducted. The mean grid size of  $10 \mu$ m is sufficient to

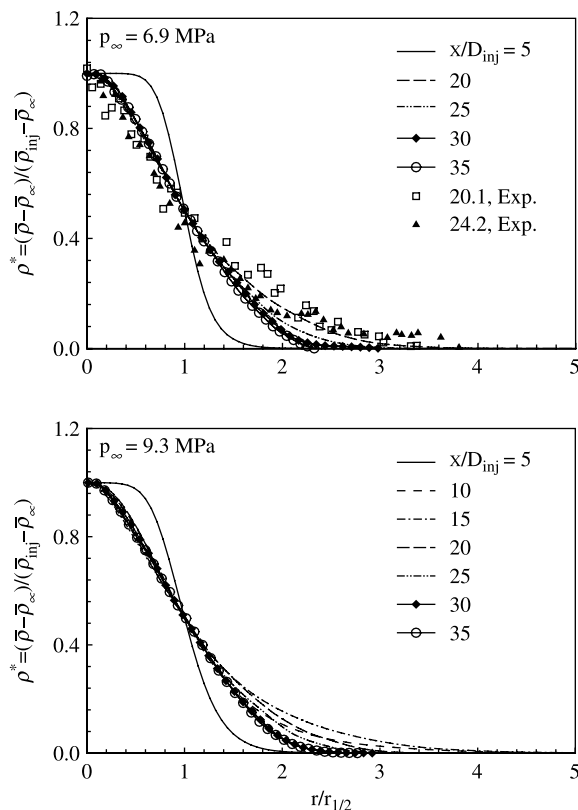


Figure 4. Radial distributions of normalized density at different axial locations ( $T_\infty = 300$  K,  $u_{inj} = 15$  m/s,  $T_{inj} = 120$  K,  $D_{inj} = 254$   $\mu$ m).

resolve the inertial sub-range of the TKE spectrum estimated based on the inlet Reynolds number of the oxygen stream. The physical time step is  $0.5 \times 10^{-3}$  ms and the maximum CFL number for the inner-loop pseudo-time integration is 0.7. A more detailed description of the simulation conditions is given in Zong and Yang (2006, 2007).

Figure 6 presents close-up views of the vorticity, temperature, oxygen mass fraction, and compressibility-factor fields near the injector without chemical reactions. Three shear layers are clearly observed: one emerging from the inner rim of the LOX post; and two from the inner and outer edges of the methane annulus. A series of

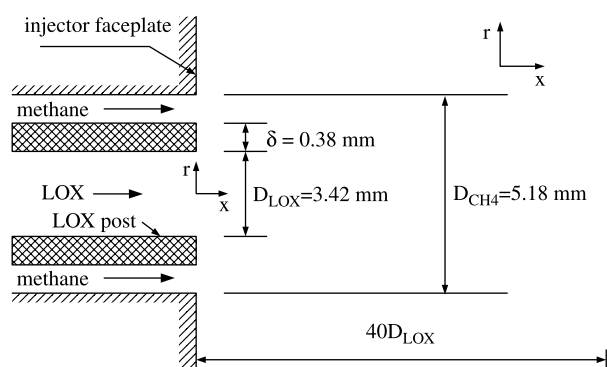


Figure 5. Schematic diagram of shear-coaxial injection of oxygen and methane.

large-scale vortices shed from the outer rim of the LOX post. As those vortices develop, the two shear layers separated by the LOX post merge. Although those energetic eddies concentrate on the light fluid side, they entrain the denser oxygen much deep into the methane stream and greatly facilitate the mixing process.

The situation with chemical reactions is also considered. LOX and methane are injected at temperatures of 122 and 300 K, respectively. The bulk velocities of the two streams are 13 and 75 m/s, respectively. The mixture and momentum-flux ratios are 3 and 2.5, respectively. The injection conditions are typical of operational liquid-propellant rocket engines. The combustion chamber is preconditioned with a mixture of  $\text{CO}_2$  and  $\text{H}_2\text{O}$  at the stoichiometric ratio and 1800 K. The ambient pressure is fixed at 100 atm. A one-step global chemical kinetics model for methane and oxygen is employed (Westbrook and Dryer 1981).

Figure 7 shows snapshots of vorticity, temperature, methane mass fraction, and compressibility-factor fields. A diffusion-dominated flame emanates immediately from the LOX post and propagates downstream along the surface of the LOX stream. A wake region, which consists of hot combustion products, effectively separates the methane and LOX streams. Similar to the non-reacting flow case, the near-field flow dynamics are characterized by the evolution of the three mixing layers originating from the inner and outer edges of the methane annulus and the inner rim of the LOX post. The evolution of the inner mixing layer of the methane stream, however, is slightly inhibited by the expansion of the combustion products in the flame zone. Because of the strong density stratification

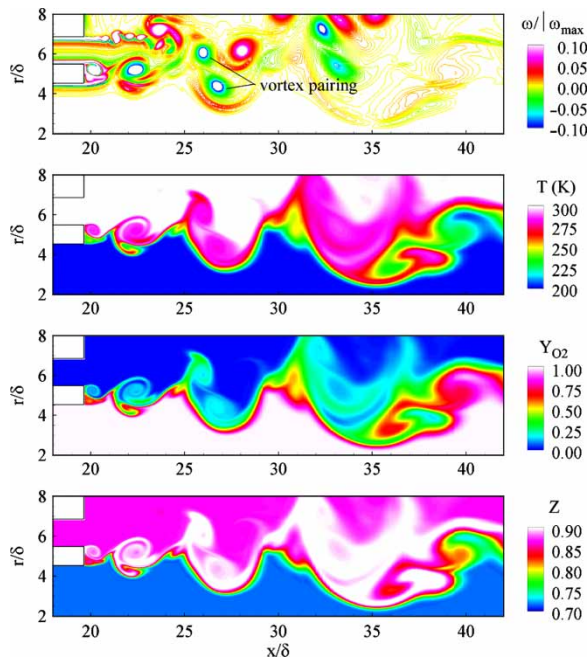


Figure 6. Snapshots of vorticity, temperature, oxygen mass fraction, and compressibility-factor fields of shear-coaxial injection of oxygen and methane ( $p_\infty = 100$  atm,  $T_{\text{O}_2} = 200$  K,  $u_{\text{O}_2} = 10$  m/s,  $T_{\text{CH}_4} = 300$  K,  $u_{\text{CH}_4} = 30$  m/s).

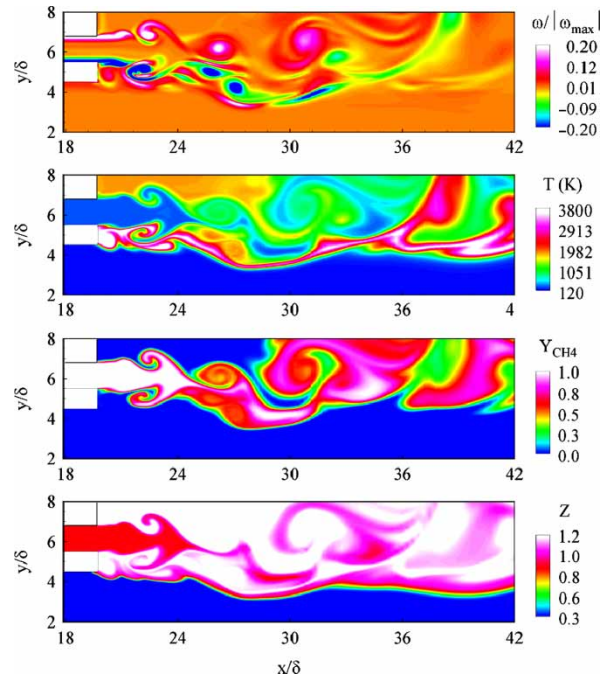


Figure 7. Snapshots of vorticity, temperature, methane mass fraction and compressibility-factor fields near the injector faceplate ( $p_\infty = 100$  atm,  $T_{\text{O}_2} = 122$  K,  $u_{\text{O}_2} = 13$  m/s,  $T_{\text{CH}_4} = 300$  K,  $u_{\text{CH}_4} = 75$  m/s).

between the oxygen stream and flame, the large-scale vortices emerging from the outer rim of the LOX post evolve in a manner analogous to that produced by a backward-facing step and mainly reside on the lighter fluid side. Consequently, the denser oxygen stream is less influenced by those vortices.

To assess the numerical performance of the present scheme, calculations are also conducted using the preconditioning scheme developed in Meng and Yang (2003) for both the non-reacting and reacting flows. The same flow solver described in Section 3 is employed, but with the preconditioning formulation based on the pressure–enthalpy type of primitive variables and a different preconditioning matrix in Meng and Yang

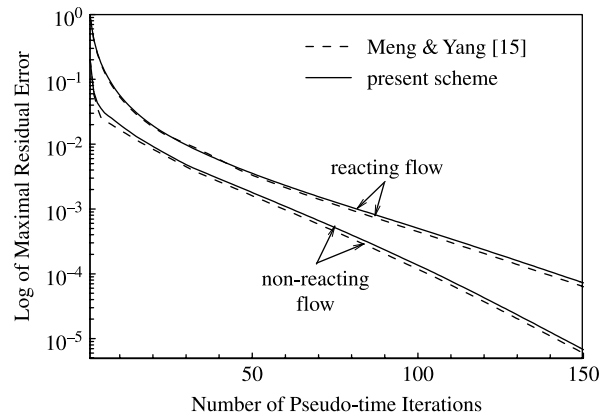


Figure 8. Convergence histories in the pseudo-time domain for shear-coaxial injection and combustion of oxygen and methane.

Table 3. CPU time per iteration in pseudo-time.

	Non-reacting flow case			Reacting flow case		
	$t_{sp}$ (s)	$t_{eos}$ (s)	$t_{eos}/t_{sp}$ (%)	$t_{sp}$ (s)	$t_{eos}$ (s)	$t_{eos}/t_{sp}$ (%)
Present scheme	52	1.8	3	87	3.8	4
Meng and Yang (2003)	120	70.0	58	158	86.0	54

(2003). The use of enthalpy as one of the dependent variables leads to an iteration solution of the real-fluid equation of state by means of the Newton-Raphson method with a convergence criterion of  $|\Delta\rho|/\rho \leq 10^{-6}$  and  $|\Delta T|/T \leq 10^{-6}$ . A relaxation of this criterion may result in an overflow of the calculation due to strong property variations in the flowfield. Figure 8 compares the convergence histories of computations using the schemes developed in the present study and in Meng and Yang (2003). Because the same temporal and spatial discretization techniques are employed, the two schemes exhibit an almost identical behaviour of convergence in terms of the number of pseudo-time iterations. The present scheme, however, is much more efficient because it avoids laborious iterations in determining temperature from enthalpy. Table 3 lists the CPU times per pseudo-time iteration,  $t_{sp}$ , and the times for solving the equation of state,  $t_{eos}$ . All the computations were performed on a Pentium IV 2.4 GHz processor. Less than 5% of the total CPU usage is expended for solving the equation of state with the present scheme, as opposed to more than 50% in the scheme in Meng and Yang (2003). The overall computational time is also reduced by half. Another major benefit of the present scheme is that the computational burden for each spatial grid cell is the same because no iterations are required for solving the equation of state. The load balance among numerical blocks is much easier to achieve on a distributed computing facility.

## 6. Conclusions

A general treatment of real-fluid thermodynamics within the framework of a preconditioning scheme has been established. All of the numerical properties are derived directly from fundamental thermodynamics theories based on the concepts of partial-mass and partial-density properties. The algorithm is self-consistent and robust, and can accommodate any equation of state for fluid mixtures. The scheme employs temperature instead of enthalpy as the primary dependent variable in the preconditioned energy equation. As a consequence, the laboriously iterative solution of the equation of state can be avoided. The computational burden is uniform throughout the entire domain. A series of sample calculations, including the injection and combustion of cryogenic fluids under supercritical conditions, were conducted to assess the effectiveness of the scheme at various fluid states. In addition, a numerical stability

analysis was performed to characterize the algorithm behaviour over a broad range of flow conditions.

## Acknowledgements

This work was partly sponsored by the Air Force Office of Scientific Research under Grant No. FA 9550-07-1-0111, and partly sponsored by NASA through the Constellation University Institutes Project (CUIP) Grant. The authors gratefully acknowledge the support and advice given by Mitat Birkan, Claudia Meyer, Jeff Rybak and Kevin Tucker.

## References

- Buelow, P.E.O., Venkateswaran, S. and Merkle, C.L., Effect of grid aspect ratio on convergence. *AIAA J.*, 1994, **32**, 2401–2408.
- Chehroudi, B., Talley, D. and Coy, E., Visual characteristics and initial growth rates of round cryogenic jets at subcritical and supercritical pressures. *Phys. Fluids*, 2002a, **14**, 850–861.
- Chehroudi, B., Cohn, R., Talley, D. and Badakhshan, A., Cryogenic shear layers: experiments and phenomenological modeling of the initial growth rate under subcritical and supercritical conditions. *Int. J. Heat Fluid Flow*, 2002b, **23**, 554–563.
- Choi, Y.H. and Merkle, C.L., The application of preconditioning to viscous flows. *J. Comput. Phys.*, 1993, **105**, 207–223.
- Darmofal, D. and Van Leer, B., *Local Preconditioning: Manipulating Mother Nature to Fool Father Time, Computing the Future II: Advances and Prospects in Computational Aerodynamics*, edited by M. Hafez and D. Caughey, 1998 (Wiley: New York).
- Edwards, J.R. and Liou, M.S., Low-diffusion flux-splitting scheme for flows at all speeds. *AIAA J.*, 1998, **36**, 1610–1617.
- Edwards, J.R., Franklin, R.K. and Liou, M.S., Low-diffusion flux-splitting methods for real fluid flows with phase transitions. *AIAA J.*, 2000, **38**, 1624–1633.
- Ely, J.F. and Hanley, H.J., Prediction of transport properties. 1. Viscosity of fluids and mixtures. *Ind. Eng. Chem. Fundam.*, 1981, **20**, 323–332.
- Ely, J.F. and Hanley, H.J., Prediction of transport properties. 2. Thermal conductivity of pure fluids and mixtures. *Ind. Eng. Chem. Fundam.*, 1983, **22**, 90–97.
- Erlebacher, G., Hussaini, M.Y., Speziale, C.G. and Zang, T.A., Toward the large eddy simulation of compressible turbulent flows. *J. Fluid Mech.*, 1992, **238**, 155–185.
- Graboski, M.S. and Daubert, T.E., A modified Soave equation of state for phase equilibrium calculation. 1. Hydrocarbon systems. *Ind. Eng. Chem. Proc. Des. Dev.*, 1978, **17**, 448–454.
- Graboski, M.S. and Daubert, T.E., A modified Soave equation of state for phase equilibrium calculation. 1. Systems containing hydrogen. *Ind. Eng. Chem. Proc. Des. Dev.*, 1979, **18**, 300–305.
- Guillard, H. and Viozat, C., On the behavior of upwind scheme in the low Mach number limit. *Comput. Fluids*, 1999, **28**, 63–86.
- Hsieh, S.Y. and Yang, V., A preconditioned flux-differencing scheme for chemically reacting flows at all Mach numbers. *Int. J. Comput. Fluid Dyn.*, 1997, **8**, 31–49.
- Jacobsen, R.T. and Stewart, R.B., Thermodynamic properties of nitrogen including liquid and vapor phases from 63 K to 2000K with pressure to 10,000 bar. *J. Phys. Chem. Ref. Data*, 1973, **2**, 757–922.
- Jameson, A., The evolution of computational methods in aerodynamics. *J. Appl. Math.*, 1983, **50**, 1052–1070.

- Jorgenson, P. and Turkel, E., Central difference TVD schemes for time dependent and steady state problems. *J. Comput. Phys.*, 1993, **107**, 297–308.
- Mao, D., Edwards, J.R., Kuznetsov, A.V. and Srivastava, R.K., Development of low-diffusion flux-splitting methods for dense gas-solid flows. *J. Comput. Phys.*, 2003, **185**, 100–119.
- Meng, H. and Yang, V., A unified treatment of general fluid thermodynamics and its application to a preconditioning scheme. *J. Comput. Phys.*, 2003, **189**, 277–304.
- Meng, H., Hsiao, G.C., Yang, V. and Shuen, J.S., Transport and dynamics of liquid oxygen droplets in supercritical hydrogen streams. *J. Fluid Mech.*, 2005, **527**, 115–139.
- Merkle, C.L., Sullivan, J.Y., Buelow, P.E.O. and Venkateswaran, S., Computation of flows with arbitrary equation of state. *AIAA J.*, 1998, **36**, 515–521.
- Moran, M.J. and Shapiro, H.N., *Fundamentals of Engineering Thermodynamics*, 4th ed., 1999 (John Wiley & Sons, Inc. : New York).
- Oefelein, J.C., Mixing and combustion of cryogenic oxygen-hydrogen shear-coaxial jet flames at supercritical pressure. *Combust. Sci. Tech.*, 2006, **178**, 229–252.
- Oefelein, J.C. and Yang, V., Modeling high-pressure mixing and combustion processes in liquid rocket engines. *J. Prop. Power*, 1998, **14**, 843–857.
- Rai, M.M. and Chakravarthy, S., Conservative high-order accurate finite difference methods for curvilinear grids, AIAA Paper No. 1993-3380 1993.
- Shuen, J.S., Chen, K.H. and Choi, Y.H., A coupled implicit method for chemical non-equilibrium flows at all speeds. *J. Comput. Phys.*, 1993, **106**, 306–318.
- Swanson, R.C. and Turkel, E., On central difference and upwind schemes. *J. Comput. Phys.*, 1992, **101**, 292–306.
- Takahashi, S., Preparation of a generalized chart for diffusion coefficients of gases at high pressures. *J. Chem. Eng (Japan)*, 1974, **7**, 417–420.
- Turkel, E., Robust low speed preconditioning for viscous high lift flows, AIAA Paper No. 2002-0962 2002.
- Turkel, E., Preconditioned methods for solving the incompressible and low speed compressible equations. *J. Comput. Phys.*, 1987, **72**, 277–298.
- Turkel, E., Preconditioning techniques in computational fluid dynamics. *Annu. Rev. Fluid Mech.*, 1999, **31**, 385–416.
- Turkel, E. and Vatsa, V.N., Choice of variables and preconditioning for time dependent problems, AIAA paper No. 2003-3692 2003.
- Venkateswaran, S., Merkle, C.L., Zeng, X. and Li, D., Influence of large-scale pressure changes on preconditioned solutions at low speeds. *AIAA J.*, 2004, **42**, 2490–2498.
- Weiss, J.M. and Smith, W.A., Preconditioning applied to variable and constant density flows. *AIAA J.*, 1995, **33**, 2050–2057.
- Westbrook, C.K. and Dryer, F.L., Simplified reaction for the oxidation of hydrocarbon fuels in flames. *Combust. Sci. Tech.*, 1981, **27**, 31–43.
- Yang, V., Modeling of supercritical vaporization, mixing, and combustion processes in liquid-fueled propulsion systems. *Proc. Combust. Inst.*, 2000, **28**, 925–942.
- Zong, N. and Yang, V., Cryogenic jets and mixing layers in transcritical and supercritical environments. *Combust. Sci. Tech.*, 2006, **178**, 193–227.
- Zong, N. and Yang, V., Near-field flow and flame dynamics of LOX/methane shear-coaxial injector under supercritical conditions. *Proc. Combust. Inst.*, 2007, **31**, 2309–2317.
- Zong, N., Meng, H., Hsieh, S.Y. and Yang, V., A numerical study of cryogenic fluid injection and mixing under supercritical conditions. *Phys. Fluids*, 2004, **16**, 4248–4261.

## A Appendix A

The Jacobian matrices,  $T \equiv \partial Q/\partial \hat{Q}$ ,  $A \equiv \partial E/\partial \hat{Q}$ ,  $B \equiv \partial F/\partial \hat{Q}$  and  $D \equiv \partial S/\partial \hat{Q}$  are derived as:

$$T = \begin{pmatrix} \frac{1}{A_p} & 0 & 0 & -\frac{A_T}{A_p} & -\frac{A_{Y_1}}{A_p} & \dots & -\frac{A_{Y_{N-1}}}{A_p} \\ \frac{u}{A_p} & \rho & 0 & -\frac{A_T u}{A_p} & -\frac{A_{Y_1} u}{A_p} & \dots & -\frac{A_{Y_{N-1}} u}{A_p} \\ \frac{v}{A_p} & 0 & \rho & -\frac{A_T v}{A_p} & -\frac{A_{Y_1} v}{A_p} & \dots & -\frac{A_{Y_{N-1}} v}{A_p} \\ \frac{h_u}{A_p} + \left( \sum_{i=1}^N Y_i \tilde{e}_i - e - \frac{p}{\rho} \right) \left( \frac{\partial \rho}{\partial p} \right)_{T, Y_i} & \rho u & \rho v & \rho B_T - \frac{A_T e_t}{A_p} & \rho B_{Y_1} - \frac{A_{Y_1} e_t}{A_p} & \dots & \rho B_{Y_{N-1}} - \frac{A_{Y_{N-1}} e_t}{A_p} \\ \frac{Y_1}{A_p} & 0 & 0 & -\frac{A_T Y_1}{A_p} & \rho - \frac{A_{Y_1} Y_1}{A_p} & \dots & -\frac{A_{Y_{N-1}} Y_1}{A_p} \\ \vdots & \vdots & \vdots & \vdots & \vdots & \ddots & \vdots \\ \frac{Y_{N-1}}{A_p} & 0 & 0 & -\frac{A_T Y_{N-1}}{A_p} & -\frac{A_{Y_1} Y_{N-1}}{A_p} & \dots & \rho - \frac{A_{Y_{N-1}} Y_{N-1}}{A_p} \end{pmatrix} \quad (\text{A.1})$$

$$A = \begin{pmatrix} \frac{u}{A_p} & \rho & 0 & -u \frac{A_T}{A_p} & -u \frac{A_{Y_1}}{A_p} & \dots & -u \frac{A_{Y_{N-1}}}{A_p} \\ 1 + \frac{u^2}{A_p} & 2\rho u & 0 & -u^2 \frac{A_T}{A_p} & -u^2 \frac{A_{Y_1}}{A_p} & \dots & -u^2 \frac{A_{Y_{N-1}}}{A_p} \\ \frac{uv}{A_p} & \rho v & \rho u & -uv \frac{A_T}{A_p} & -uv \frac{A_{Y_1}}{A_p} & \dots & -uv \frac{A_{Y_{N-1}}}{A_p} \\ \frac{u}{A_p} \left[ h_t + \left( \sum_{i=1}^N Y_i \tilde{e}_i - e - \frac{p}{\rho} \right) + 1 \right] & h_t + \rho u^2 & \rho uv & u \left( \rho B_T - \frac{A_T e_t}{A_p} \right) & u \left( \rho B_{Y_1} - \frac{A_{Y_1} e_t}{A_p} \right) & \dots & u \left( \rho B_{Y_{N-1}} - \frac{A_{Y_{N-1}} e_t}{A_p} \right) \\ \frac{u Y_1}{A_p} & \rho Y_1 & 0 & -u \frac{A_T Y_1}{A_p} & u \left( \rho - \frac{A_{Y_1} Y_1}{A_p} \right) & \dots & -u \frac{A_{Y_{N-1}} Y_1}{A_p} \\ \vdots & \vdots & \vdots & \vdots & \vdots & \ddots & \vdots \\ \frac{u Y_{N-1}}{A_p} & \rho Y_{N-1} & 0 & -u \frac{A_T Y_{N-1}}{A_p} & -u \frac{A_{Y_1} Y_{N-1}}{A_p} & \dots & u \left( \rho - \frac{A_{Y_{N-1}} Y_{N-1}}{A_p} \right) \end{pmatrix} \quad (\text{A.2})$$

$$B = \begin{pmatrix} \frac{v}{A_p} & 0 & \rho & -v \frac{A_T}{A_p} & -v \frac{A_{Y_1}}{A_p} & \dots & -v \frac{A_{Y_{N-1}}}{A_p} \\ \frac{uv}{A_p} & \rho v & \rho u & -uv \frac{A_T}{A_p} & -uv \frac{A_{Y_1}}{A_p} & \dots & -uv \frac{A_{Y_{N-1}}}{A_p} \\ 1 + \frac{v^2}{A_p} & 0 & 2\rho v & -v^2 \frac{A_T}{A_p} & -v^2 \frac{A_{Y_1}}{A_p} & \dots & -v^2 \frac{A_{Y_{N-1}}}{A_p} \\ \frac{v}{A_p} \left[ h_t + \left( \sum_{i=1}^N Y_i \tilde{e}_i - e - \frac{p}{\rho} \right) + 1 \right] & \rho uv & h_t + \rho v^2 & v \left( \rho B_T - \frac{A_T e_t}{A_p} \right) & v \left( \rho B_{Y_1} - \frac{A_{Y_1} e_t}{A_p} \right) & \dots & v \left( \rho B_{Y_{N-1}} - \frac{A_{Y_{N-1}} e_t}{A_p} \right) \\ \frac{v Y_1}{A_p} & 0 & \rho Y_1 & -v \frac{A_T Y_1}{A_p} & v \left( \rho - \frac{A_{Y_1} Y_1}{A_p} \right) & \dots & -v \frac{A_{Y_{N-1}} Y_1}{A_p} \\ \vdots & \vdots & \vdots & \vdots & \vdots & \ddots & \vdots \\ \frac{v Y_{N-1}}{A_p} & 0 & \rho Y_{N-1} & -v \frac{A_T Y_{N-1}}{A_p} & -v \frac{A_{Y_1} Y_{N-1}}{A_p} & \dots & v \left( \rho - \frac{A_{Y_{N-1}} Y_{N-1}}{A_p} \right) \end{pmatrix} \quad (\text{A.3})$$

$$D = \begin{pmatrix} 0 & 0 & 0 & 0 & 0 & \dots & 0 \\ 0 & 0 & 0 & 0 & 0 & \dots & 0 \\ 0 & 0 & 0 & 0 & 0 & \dots & 0 \\ 0 & 0 & 0 & 0 & 0 & \dots & 0 \\ \left( \frac{\partial \omega_1}{\partial p} \right)_{T, Y_i} & 0 & 0 & \left( \frac{\partial \omega_1}{\partial T} \right)_{p, Y_i} & \left( \frac{\partial \omega_1}{\partial Y_1} \right)_{p, T, Y_{j \neq 1}} & \vdots & \left( \frac{\partial \omega_1}{\partial Y_{N-1}} \right)_{p, T, Y_{j \neq N-1}} \\ \vdots & \vdots & \vdots & \vdots & \vdots & \ddots & \vdots \\ \left( \frac{\partial \omega_{N-1}}{\partial p} \right)_{T, Y_i} & 0 & 0 & \left( \frac{\partial \omega_{N-1}}{\partial T} \right)_{p, Y_i} & \left( \frac{\partial \omega_{N-1}}{\partial Y_1} \right)_{p, T, Y_{j \neq 1}} & \dots & \left( \frac{\partial \omega_{N-1}}{\partial Y_{N-1}} \right)_{p, T, Y_{j \neq N-1}} \end{pmatrix} \quad (\text{A.4})$$